

TOWARDS THE NUMERICAL MODELLING OF RESIDUAL SEABED LIQUEFACTION USING OPENFOAM

RANJITH KHUMAR SHANMUGASUNDARAM^{1,2,*}, HENRIK RUSCHE¹, CHRISTIAN WINDT², V.S.ÖZGÜR KIRCA^{3,4}, B.MUTLU SUMER³ AND NILS GOSEBERG²,

¹ WIKKI GESELLSCHAFT FÜR NUMERISCHE KONTINUUMSMECHANIK MBH, WERNIGERODE , GERMANY

²LEICHTWEISS-INSTITUTE FOR HYDRAULIC ENGINEERING AND WATER RESOURCES, TU BRAUNSCHWEIG, GERMANY

³ BM SUMER CONSULTANCY & RESEARCH , ISTANBUL, TURKEY

⁴ DEPARTMENT OF CIVIL ENGINEERING, ISTANBUL TECHNICAL UNIVERSITY, ISTANBUL, TURKEY

Email address: r.shanmugasundaram@wikki-gmbh.de, h.rusche@wikki-gmbh.de, c.windt@tu-braunschweig.de, ozk@bmsumer.com, bms@bmsumer.com, n.goseberg@tu-braunschweig.de

DOI: 10.51560/ofj.v2.56

Version(s): foam-extend 4.1

Repo: <https://github.com/NuLIMAS/pressureBuildupFoam>

ABSTRACT. Knowledge of the interaction between free surface waves and the seabed is required for the reliable design of marine structures, preventing severe structural failures. To that end, this paper presents the numerical modelling of wave-induced residual liquefaction of seabed soil. An OpenFOAM® finite volume solver is developed to simulate the behaviour of pore pressure and shear stress in the soil and is validated against analytical reference data. The soil is considered as a poro-elastic solid and an additional equation is solved for the pore pressure buildup. The governing equations are valid only up to the onset of liquefaction. A criterion based on the accumulated pore pressure is applied in order to predict the onset of residual liquefaction. The results show that the pore pressure and shear stresses are in good agreement with the analytical results and the relative errors are less than three percent. Also, the numerical results indicate that the wave induced residual liquefaction originates from the mudline and progresses slowly down the soil which is consistent with the analytical results. The pore pressure buildup for a seabed with stone columns shows that the liquefaction potential is very low near the stone column.

Keywords: *poro-elastic solid, accumulated pore pressure, residual liquefaction, finite volume method, offshore structures*

1. INTRODUCTION

Seabed liquefaction is the phenomenon by which the seabed soil loses its strength and stiffness due to the accumulation of pore pressure and behaves like a highly viscous fluid [1]. The liquefaction process is triggered by stresses acting on the seabed, which, in turn, can be induced by cyclic wave action or seismic loading. Essentially, when excess pore pressures equal the effective stresses within the soil matrix, an increase in external forces can no longer be born and soil liquefaction is initiated [2].

During the shearing, the grains in loosely packed soils rearrange. As a result of the induced shear force, the grain skeleton of the soil has a tendency to contract and thus decrease the void space, or pore volume, within the soil. This results in increasing pore pressure and the tendency of the water to flow out. If drainage is possible, there is a decrease in the void space and dissipation of the pore pressure. If undrained, the pore pressure will remain high. By Terzaghi's principle, this results in reduced effective stress in a soil column, which makes it more prone to start sliding by the applied external shear force. After the onset of sliding, the soil behaves like a highly viscous non-Newtonian fluid – it liquefies. By ongoing granular collisions and entertainment of ambient water, Figure 1b is obtained after some time.

More specifically, liquefaction can be mainly grouped into two categories: (i) residual liquefaction, and (ii) momentary liquefaction. Residual liquefaction occurs when the accumulated pore pressure overcomes the initial mean normal effective stress, resulting in completely unbound soil particles [4]. Momentary liquefaction generally occurs when a transient upward pore pressure gradient, induced by wave troughs, overcomes the initial vertical effective stress [5]. This momentary liquefaction is a relatively short-lived

* Corresponding author

Received: 30 September 2021, Accepted: 26 March 2022, Published: 21 May 2022

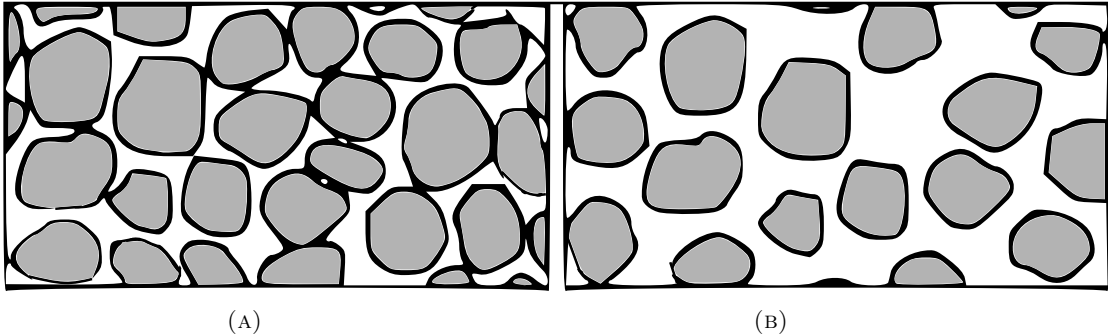


FIGURE 1. In (A), water fills the space between soil grains but the contact between the grains still holds the sediment together. In (B), liquefaction resulted in unbound soil grains allowing the sediment to flow like liquid. Redrawn from [3]

phenomenon and will not be further considered in this paper. Therefore, this study only concerns the wave-induced residual liquefaction.

With the increasing exploitation of the marine environment, the liquefaction around marine structures renders an important topic in the field of coastal and offshore engineering. Seabed liquefaction can eventually lead to the severe failure of marine structures, such as buried pipelines or breakwaters. Some of the examples of these failures are pipeline failure reported by Christian *et al.* [6], breakwater failure reported by Lundgren *et al.* [7] and sinking failure of Drag Embedment anchors reported by Kirca and Sumer [8]. More recently, the analysis of liquefaction around offshore renewable energy systems, in particular with regard to anchors of floating offshore wind structures, gained increasing interest [9].

The offshore wind industry is progressing towards the commercialisation of floating offshore wind turbines (FOWT) at locations with deep water depths (> 50 m) to further exploit the capacity of offshore wind. During operation, the station keeping of such FOWTs using mooring systems is crucial. One approach for the design of such a mooring system is the use of tension-leg type systems with gravity anchors [10, 11] (see Figure 2a). Additional complexity is added to the loading conditions of seabed soil when anchor systems are using suction bucket or caisson technology, which locally introduces negative pore pressures beneath the foundation elements [12]. For a cost-efficient and durable design of such marine structures, detailed knowledge of the hydro-geotechnical processes is required. However, gaining this knowledge is a challenging task due to the occurring (non-linear) wave–structure–soil interaction (WSSI).

A number of studies can be found in the literature which investigate the liquefaction around marine structures analytically, experimentally, and numerically. Biot's poro-elasticity theory [13] was the basis for many analytical and numerical approaches. The model allows closed analytical solution for a number of relevant cases to obtain wave-induced pore pressure, displacement, and effective stress in the soil. Yamamoto [14] and Madsen [15] were the first to represent soil as a porous medium and develop an analytical solution for wave induced seabed response using Biot's poro-elasticity. The studies have been carried out for isotropic [14] and anisotropic homogenous seabed [15]. Later, Hsu and Jeng [5, 16] studied the seabed response for a non-homogenous seabed with varying permeability and also different liquefaction criteria for momentary liquefaction. Sumer *et al.* [17] experiments showed that the process of buildup of pressure in irregular waves is much similar as in the case of regular waves. A comprehensive review of the analytical approaches to model the wave induced seabed response can be found in [18].

Jeng [18] also includes a review of different experimental tests, conducted to evaluate the wave-induced seabed response. Three different experimental techniques are usually used: i) Wave tank experiments, which are normally used by coastal engineers; ii) Compression tests, which are commonly used by geo-technical engineers; iii) Centrifugal wave modelling, which is again commonly used by geo-technical engineers. Each of the three techniques has its specific advantages and disadvantages. For a detailed review of the different experimental approaches, the interested reader is referred to [18] and [4].

Additionally, the numerical modelling of seabed liquefaction can provide valuable insights into the prevailing WSSI. To that end, e.g. Elsafti and Oumeraci [19] or Li *et al.* [20] propose different modelling frameworks, implemented in the open source CFD toolbox OpenFOAM®. In these works, finite-volume method (FVM)-based quasi-steady models are applied to solve the physics of poro-elasticity and the numerical results are validated against experimental results of a standing wave-induced seabed response near a vertical wall. In addition, Li *et al.* [20] describe different liquefaction criteria used for the prediction

of the onset of momentary liquefaction. Also, Li *et al.* [21] proposed a numerical model for scour beneath sub sea structures, considering the effect of upward seepage in the seabed. In both studies, the dynamic wave forces are modelled based on the waves2foam toolbox [22] in conjunction with the Volume of Fluid (VOF) method.

While both the numerical models in [19] and [20] can be applied to predict the onset of momentary liquefaction, none of the models is capable of accounting for pore pressure buildup or the behaviour of soil after the liquefaction.

Duan *et al.* [23, 24] and Sui *et al.* [25] studied the residual seabed response to hydrodynamic loadings near a monopile. Duan *et al.* [23, 24] developed a three-dimensional numerical model for residual liquefaction in the vicinity of a mono-pile, considering both waves and currents. Here, the wave and current interactions are modelled using IHFoam, in which the flow is modeled using volume-averaged Reynolds-Averaged Navier-Stokes (VRANS) equations. In Sui *et al.* [25], the wave loading on the seabed is modelled using the Boussinesq approximation. Both Duan *et al.* and Sui *et al.* use a liquefaction criterion based on the accumulated pore pressure to predict the onset of residual liquefaction. While the models are capable of predicting the accumulated pore pressure, the behaviour of the liquefied soil can not be simulated.

Based on the reviewed literature, an OpenFOAM® -based modelling framework needs to be developed to represent residual liquefaction, which also includes soil modelling after liquefaction until compaction, in order to overcome the drawbacks of existing numerical modelling tools. The present paper serves as a stepping stone towards such a model with a focus only until the onset of liquefaction. Post-liquefaction and soil compaction modelling will be the part of future work.

On the basis of an idealised representation of an offshore floating platform (see Figure 2a), such a model would embrace three different regions (see Figure 2b): the waves above the seabed (Ω_1), the solid soil region (Ω_2), and, finally, the liquefied region, i.e. the region in which the soil behaves as non-Newtonian fluid (Ω_3). In addition, an idealised gravity anchor is placed on the seabed and is treated as a rigid body with six degrees of freedom.

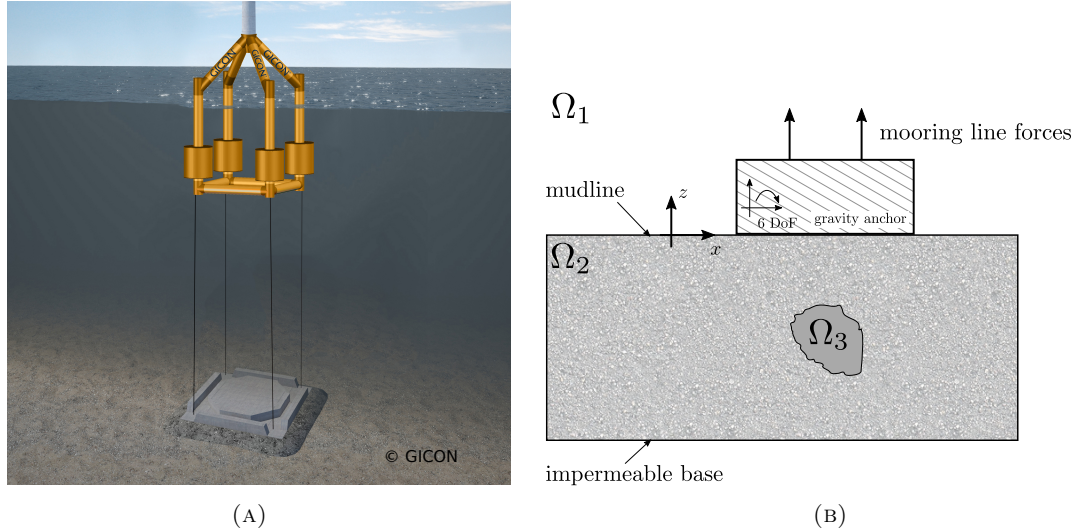


FIGURE 2. Visualisation of a floating offshore structure with gravity anchor serving as a case study (A) [11] and an idealised schematic for the numerical model definition, with the three regions: waves above the seabed (Ω_1), solid soil (Ω_2), and liquefied soil (Ω_3) (B)

This study presents the implementation of a numerical model for the simulation of the onset of liquefaction in a poro-elastic soil. In the spirit of the above mentioned analytical solutions, the wave region (Ω_1) is replaced by an oscillating pressure boundary condition representing linear progressive waves. Using the analytical wave solutions is based on the assumption that the structure has a minor influence on the wave field. This treatment removes the need to solve for the water phase including resolution of the free surface interface. In the solid soil region (Ω_2), a common continuum approach for granular materials is adopted: isotropic poro-elastic solid with incompressible pore fluid. In this region two governing equations are solved: i) quasi steady-state pore fluid continuity yielding pore pressure, ii) quasi steady-state linear momentum yielding displacements. The liquefied and non liquefied regions can be distinguished

based on the criteria defined by Sumer [4] which states that liquefaction occurs when the accumulated pore pressure is greater than the initial mean normal effective stress in the soil (see Section 2). Once this criteria is met, the governing equations need to be solved with appropriate constitutive relations. In the following, only the onset of liquefaction is considered and the implementation of the liquefied soil behaviour is part of pertinent future work.

The remainder of the paper is structured as follows. Section 2 provides the theoretical background for numerical modelling of poro-elastic soil, including the equations to solve the pore pressure and accumulated pore pressure. In Section 3, the implementation of the governing equations in OpenFOAM® is detailed and relevant sections of the code are shown. Following on, in Section 4, two different test cases, one for the validation of the calculation of pore pressure and shear stress, one for validating the onset of liquefaction are presented and discussed. In addition, an example is shown to estimate the accumulated pore pressure for a seabed with the stone column. Finally, in Section 5, conclusions are drawn and future work is identified.

2. THEORETICAL BACKGROUND

As stated in Section 1, the soil is considered a poro-elastic solid with incompressible pore fluid. The pore pressure and stresses are the essential components to describe the poro-elastic solid. In Section 2.1, the Biot consolidation equations, which describe the physics of poro-elasticity, are detailed. In Section 2.2, an equation is introduced which describes the pore pressure buildup.

2.1. Biot's consolidation equations. The Biot equations [13] govern the physics of poro-elasticity. In this work, the Biot equations are used to describe the soil stresses induced by waves. The basic assumptions of the soil for the formulation of the Biot consolidation equations are

- (1) isotropic soil behaviour
- (2) stress-strain relationships can be reversed under final equilibrium conditions
- (3) linear stress-strain relation
- (4) small strains
- (5) compressible pore fluid consisting of incompressible water and entrapped compressible air
- (6) Darcy flow of the pore water

Based on these assumptions, two equations are derived to represent the pore fluid continuity and linear momentum balance. In this quasi-steady approach, both the acceleration of the soil skeleton and the acceleration of the pore water relative to the soil skeleton are ignored. There are two other formulations i) Partial dynamic, in which only the acceleration of the soil skeleton is considered and ii) Fully dynamic, in which both the acceleration of the soil skeleton and the acceleration of the pore water relative to the soil skeleton are considered.

2.1.1. Quasi steady-state linear momentum: The total momentum balance of the poro-elastic solid is achieved when the equilibrium conditions of the stress field are satisfied.

$$\nabla \cdot \sigma = 0, \quad (1)$$

where σ is the stress tensor. Here, the normal stress includes the normal stress carried by soil, as well as the normal stress carried by pore water. The soil constitutive model used in this work is a simple poro-elastic model. The total stress tensor (σ) for the poro-elastic solid is given by

$$\sigma = \sigma' - pI, \quad (2)$$

where σ' is the effective stress, p is the pore fluid pressure, and I is the identity tensor.

On applying Hooke's law for effective stress-strain relationship, the equilibrium of poro-elastic soil can be derived as follows,

$$G\nabla^2U + \frac{G}{1-2\nu}\nabla\epsilon = \nabla p, \quad (3)$$

where G is the shear Modulus and ν is the Poisson ratio and U is the displacement vector. Variable ϵ denotes the volume increase per unit volume of soil. In Equation (3) the left-hand side terms stem from the divergence of stress (σ' in Equation (2)). The stress tensor can be calculated in terms of displacement following

$$\sigma = G[\nabla U + (\nabla U)^T] + \lambda I * \text{tr}(\nabla U), \quad (4)$$

where λ is Lamé's constant:

$$\lambda = \frac{\nu E}{(1+\nu)(1-\nu)}, \quad (5)$$

where E is the elastic modulus.

2.1.2. *Quasi steady-state pore fluid continuity:* The conservation of mass of pore water is represented by

$$\frac{\partial}{\partial t} \left(\epsilon + \frac{n}{K'} p \right) + \nabla \cdot V = 0, \quad (6)$$

where V is the velocity vector (specific discharge), n is the porosity and K' is the true bulk modulus of elasticity of water, which is given by

$$\frac{1}{K'} = \frac{1}{K} + \frac{1 - S_r}{p_0}, \quad (7)$$

where K is the modulus of elasticity of water, S_r is the degree of saturation ($S_r = 1$ indicates that there is no air content in the soil) and p_0 is the absolute pore water pressure. In Equation (6), the term $(\frac{\partial \epsilon}{\partial t})$ represents the increase in the volume of water due to the expansion of the soil per unit volume of soil per unit time. The term $(\frac{\partial}{\partial t}(\frac{n}{K'} p))$ represents the increase in volume of water due to compressibility of water itself. As mentioned in assumption (6) above, the pore water follows Darcy's law ($V = \frac{k}{\gamma} \nabla p$). By representing the velocities in terms of pore pressure in Equation (6), the continuity equation can be derived as described in (8). In Equation (8), k represents hydraulic conductivity and γ represents specific weight of the soil.

$$\frac{k}{\gamma} \nabla^2 p = \frac{n}{K'} \frac{\partial p}{\partial t} + \frac{\partial \epsilon}{\partial t} \quad (8)$$

2.2. Pore pressure buildup. Biot's consolidation equations solve for the pore pressure and displacement but don't include the rearrangement of soil grains which is essential for the pore pressure to build up.

In order for the pore pressure to build up, Sumer [4] developed a mathematical model using a source term, f , (as a function of soil depth and time):

$$\frac{\partial P}{\partial t} = c_v \frac{\partial^2 P}{\partial z^2} + f, \quad (9)$$

where P is the accumulated pore pressure, c_v is the coefficient of consolidation, which acts as a diffusion coefficient. Equation (9) can be derived from Equations (8) and (3). Also, c_v follows from the parameters that were already introduced and is given by,

$$c_v = \frac{Gk}{\gamma} \frac{2 - 2\nu}{(1 - 2\nu) + (2 - 2\nu) \frac{nG}{K'}}. \quad (10)$$

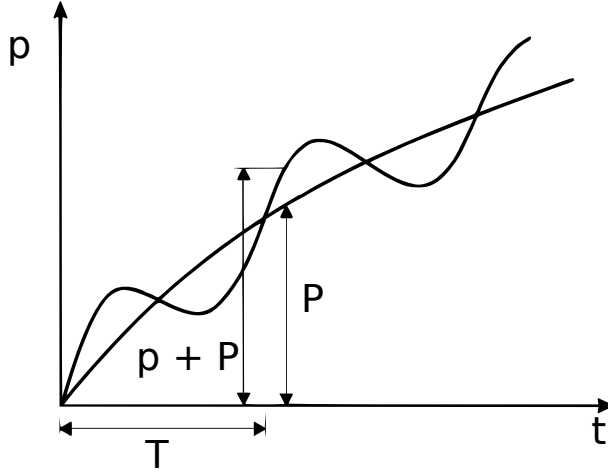


FIGURE 3. Fluctuating and mean pressure

The total pore pressure can be generally represented as sum of mean (i.e. period-averaged) and fluctuating component, $p_{\text{tot}} = P + p$, is shown in Figure 3. The fluctuating component is the pore pressure p that has been defined in Section 2.1, while the mean component is the accumulated pore pressure P . The source term f represents the total amount of averaged pore pressure generated per unit time per unit volume of soil. f can be defined as the ratio between the amount of averaged pore pressure generated and the time period, which can be represented by

$$f = \frac{\sigma'_0}{N_l T}, \quad (11)$$

where N is total number of wave cycles, N_l is the number of cycles required until onset of liquefaction, σ'_0 is the initial mean normal effective stress, and T is the wave period. The initial mean normal effective stress σ'_0 is given by

$$\sigma'_0 = \gamma'(-z) \left(\frac{1 + 2k_0}{3} \right), \quad (12)$$

where γ' is the submerged specific weight of soil, z denotes the height of seabed, and k_0 is the coefficient of lateral earth pressure. Following Peacock and Seed [26], N_l can be modelled as

$$N_l = \left(\frac{1}{\alpha} \frac{A_\tau}{\sigma'_0} \right)^{\frac{1}{\beta}}, \quad (13)$$

where A_τ is the amplitude of the shear stress. As described in Equation (4), the stress tensor is calculated from the displacement and is an instantaneous quantity. To calculate the pore pressure build up, the amplitude of the shear stress is required. In this work, A_τ is calculated from the root-mean-square of the shear stress, τ_{rms} . This can be described mathematically as follows,

$$\tau_{rms} = \sqrt{\frac{1}{T} \int_0^T (\tau(t) - \bar{\tau})^2 dt}, \quad (14)$$

where $\bar{\tau}$ is the mean shear stress and $\tau(t)$ the instantaneous shear stress. Considering the instantaneous shear stress as a simple sine wave,

$$\tau(t) = A_\tau \sin(\omega t), \quad (15)$$

where $\omega = 2\pi/T$ is the frequency. By substituting the instantaneous shear stress in Equation (14) and evaluating the integral, the relation between τ_{rms} and A_τ can be derived:

$$\tau_{rms} = \sqrt{\frac{A_\tau^2}{2}} \implies A_\tau = \sqrt{2}\tau_{rms}. \quad (16)$$

In Equation (13), α and β denote empirical coefficients, defined as a function of relative soil density, D_r , [27]:

$$\alpha = 0.34D_r + 0.087, \quad \beta = 0.37D_r - 0.46, \quad (17)$$

with

$$D_r = \frac{e_{max} - e}{e_{max} - e_{min}}, \quad (18)$$

where e , e_{max} , and e_{min} denoting the void ratio, maximum void ratio, and minimum void ratio of the soil, respectively. The void ratio can be expressed in terms of the porosity, n , following $e = n/(1-n)$.

Residual liquefaction sets in when the accumulated pore pressure is larger than the initial mean normal effective stress, which can be represented formally as,

$$\frac{P}{\sigma'_0} > 1. \quad (19)$$

The methodology explained above for modelling pore-water pressure buildup under progressive waves was validated against experiments conducted in a wave flume [28].

3. IMPLEMENTATION

This section presents the implementation of the Biot equations, as well as the governing equation for the pore pressure buildup, in OpenFOAM®. In Section 3.1, the procedure for the implementation of pore fluid continuity and linear momentum equations are described briefly. In Section 3.2, the procedure for implementation of the pore pressure buildup equation is detailed. The solver itself has also been uploaded as a public repository on GitHub for free download, the link can be found through [29].

3.1. biotFoam. `biotFoam` is a freely available OpenFOAM® package developed by Roenby [30]. Here, the model described in Section 2.1 has been implemented. The source code for the implementation of the pore fluid continuity and the linear momentum is shown in Listing 1 and 2, respectively. Also, in Listing 2, the calculation of the stress tensor from the instantaneous displacements are shown. Note that the pore pressure is denoted as 'p', the displacement is denoted as 'D' and the stress is denoted as 'SigmaD' in the code. In Listing 1, $Dp1$, $Dp2$ and $Dp3$ are the coefficients in the pore fluid continuity equation. These coefficients have been rearranged from [30] to resemble exactly as in Equation (8). The list of parameters that are denoted by different name/variables in the code are tabulated in Table 4. Also, in this work, multi-material interface from [31] has been included to correct the calculation of stresses at the interface of bonded materials. A new class named `poroElastic` is derived from Linear Elastic rheology and the

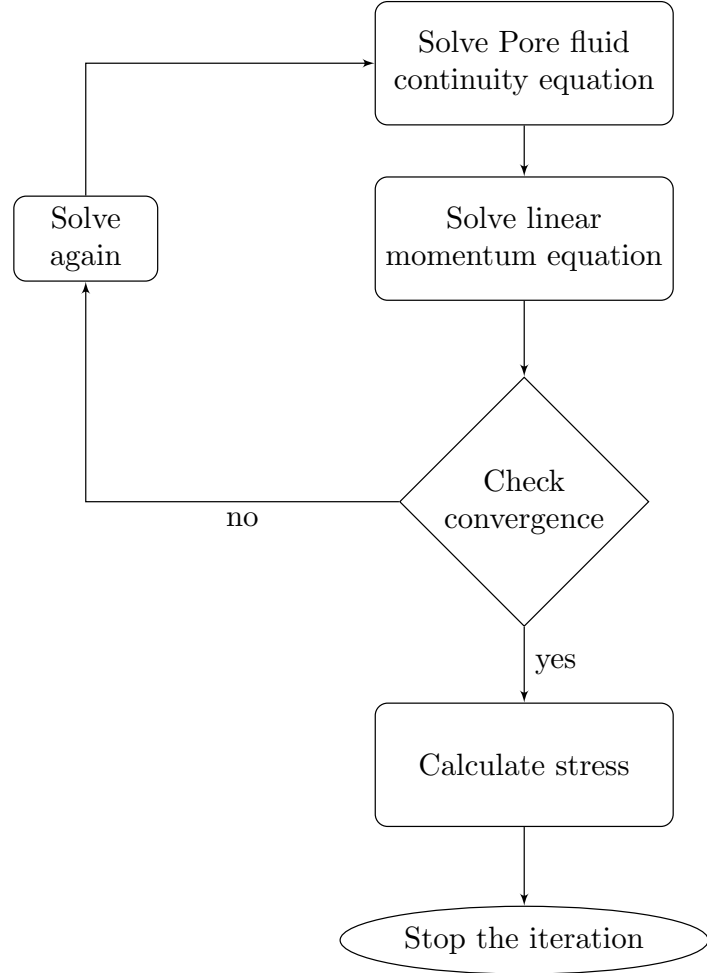


FIGURE 4. An outline of the solution procedure for a single iteration in `biotFoam`

material properties are obtained from the class. Figure 4 shows the flow chart of the solution procedure in `biotFoam`. For more details on the implementation, the interested reader is referred to [32].

```

1 // Pore fluid continuity (Equation (8))
2 solve
3 (
4   fvm::ddt(Dp1,p)
5   ==
6   fvm::laplacian(Dp2, p)
7   - fvc::div(fvc::ddt(Dp3, D))
8 );
  
```

LISTING 1. Pore fluid continuity

```

1 // Linear momentum (Equation (3))
2 solve
3 (
4   fvc::grad(p)
5   ==
6   fvm::laplacian(2*mu + lambda, D, "laplacian(DD,D)")
7   + divSigmaExp
8 );
9
10 // Stress field of type volSymmTensorField
11 sigmaD = mu*twoSymm(fvc::grad(D)) + lambda*(I*tr(fvc::grad(D)));
  
```

LISTING 2. Linear momentum

3.2. pressureBuildupFoam. `pressureBuildupFoam` is an incremental development on `biotFoam`. It adds an additional equation to solve for the pore pressure buildup. The liquefaction criteria (Equation (19)) is also implemented in this solver to predict the onset of liquefaction. Figure 5 shows the flow chart of the solution procedure in `pressureBuildupFoam`. The implementation of the additional pore pressure equation is described below.

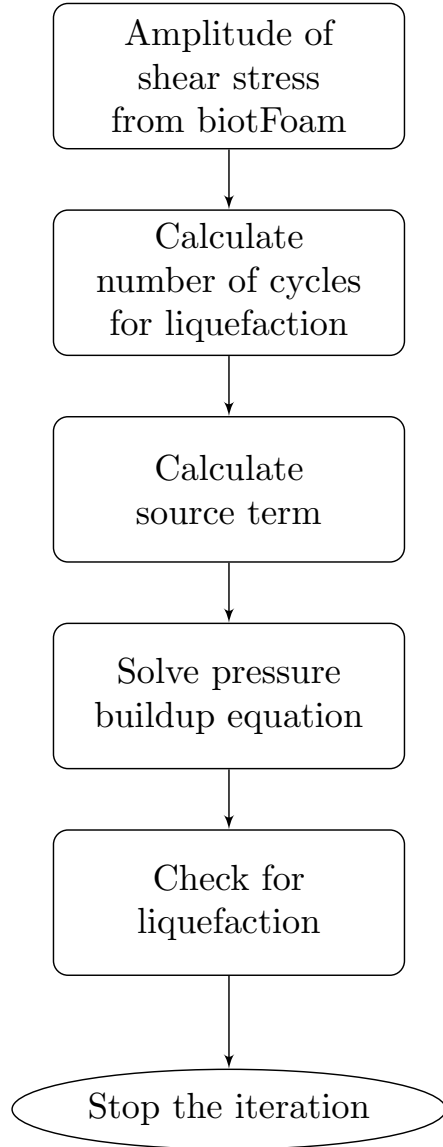


FIGURE 5. An outline of the solution procedure for a single iteration in `pressureBuildupFoam`

Equation (9) is solved to calculate the pore pressure buildup. The source term in Equation (9) depends on the initial mean normal effective stress, the number of cycles for liquefaction (amplitude of shear stress) and the time period. For the initial mean normal effective stress (Equation (12)), the submerged specific weight and the coefficient of lateral pressure needs to be explicitly defined by the user and the seabed depth can be obtained from the mesh. Similarly, for the number of cycles for liquefaction N_l (Equation (13)), the coefficients α and β can be obtained for the relative density specified by the user using the relation (17). The amplitude of the shear stress is calculated from the root-mean-square of the shear stress. The root-mean-square is not accurate until the end of one wave period, since the

mean shear stress is not accurate until one wave period. In order to overcome this issue, `biotFoam` is initially simulated to calculate the shear stress. The root-mean-square of the shear stress is calculated using OpenFOAM® function object `Prime2Mean`. The simulation is performed for a simulation time of 15 minutes to make sure that the amplitude of the shear stress is steady and accurate. This amplitude of the shear stress is then used in `pressureBuildupFoam` to calculate the source term f .

The source code for the implementation of pore pressure buildup (Equation (9)) is shown in Listing 3. Note that the accumulated pore pressure is denoted as '`pE`' in the code, as opposed to '`P`' in Section 2.2.

```

1 // Initial mean normal effective stress (Equation (12))
2 volScalarField sigma0
3 (
4     IOobject
5     (
6         "sigma0",
7         runTime.timeName(),
8         mesh,
9         IOobject::NO_READ,
10        IOobject::AUTO_WRITE
11    ),
12    gammaD*(max(mesh.C().component(vector::Z)) -
13    mesh.C().component(vector::Z))*((1.0+(2.0*k0))/3.0)
14 );
15
16
17 // Number of cycles for liquefaction (Equation (13))
18 volScalarField numCyc
19 (
20     IOobject
21     (
22         "numCyc",
23         runTime.timeName(),
24         mesh,
25         IOobject::NO_READ,
26         IOobject::AUTO_WRITE
27    ),
28    mesh,
29    dimensionedScalar("zero", dimless, 0.0),
30    zeroGradientFvPatchScalarField::typeName
31 );
32
33
34 numCyc.internalField() =
35     Foam::pow
36     (
37         (1.0/alpha)
38         *mag(tauAmp.internalField()/sigma0.internalField())
39         + SMALL, (1.0/beta)
40     );
41
42 numCyc.correctBoundaryConditions();
43
44
45 // Source term (Equation (11))
46 volScalarField f
47 (
48     IOobject
49     (
50         "f",
51         runTime.timeName(),
52         mesh,
53         IOobject::NO_READ,
54         IOobject::AUTO_WRITE
55    ),

```

```

56     sigma0/(numCyc * T),
57     zeroGradientFvPatchScalarField::typeName
58 );
59
60 f.correctBoundaryConditions();
61
62 // Pore pressure buildup (Equation (9))
63 fvScalarMatrix pEEqn
64 (
65     fvm::ddt(pE) == fvm::laplacian(cv, pE) + f
66 );
67 pEEqn.solve();

```

LISTING 3. Pore pressure buildup

3.3. Boundary conditions. In this work, the effect of waves on the seabed has been simulated by means of the pressure due to the progressive waves acting at the mudline. To that end, a new boundary condition has been developed in *biotFoam* named *progressivePressureWave* to represent the wave equation. This boundary condition is derived from the existing OpenFOAM® boundary condition *fixedValue*. The progressive wave equation can be formulated as

$$y = A \cos(mx - \omega t), \quad (20)$$

where y can be any arbitrary quantity, for example pressure, displacement etc., A is the amplitude, ω is the frequency of the wave, t is the time, and $m = 2\pi/\lambda$ is the wave number. The implementation of this boundary condition is shown in Listing 4. Note that the wave number is denoted as k_- in the code (see Listing 4), as opposed to m in Equation (20).

```

1 void Foam::propagatingPressureWaveFvPatchScalarField::updateCoeffs()
2 {
3     if (updated())
4     {
5         return;
6     }
7     scalar pi = acos(-1.0);
8
9     k_- = (2.0*pi/lambda_-)*k_-/mag(k_-);
10
11    const vectorField& x = patch().Cf();
12
13    scalar omega = 2.0*pi/T_-;
14
15    const scalar t = db().time().value();
16
17    operator==(A_-*cos((k_- & x) - omega*t));
18
19    fixedValueFvPatchField<scalar>::updateCoeffs();
20 }

```

LISTING 4. Progressive pressure wave

In addition to the pressure boundary condition, a traction free displacement boundary is implemented at the mudline. The traction force, f_{trac} , can be represented as

$$f_{trac} = \sigma \cdot \mathbf{n}, \quad (21)$$

where \mathbf{n} denotes the normal vector.

For a displacement boundary condition, the gradient boundary can be derived from the traction force by representing stress in terms of displacement [33] as shown below:

$$f_{trac} = \sigma \cdot \mathbf{n} = [G(\nabla U) + G(\nabla U)^\top + \lambda I \operatorname{tr}(\nabla U)] \cdot \mathbf{n} \quad (22)$$

$$= [(2G + \lambda)\nabla u + G(\nabla U)^\top + \lambda I \operatorname{tr}(\nabla U) - (G + \lambda)\nabla U] \cdot \mathbf{n} \quad (23)$$

$$(\nabla U) \cdot \mathbf{n} = \frac{f_{trac} - [G(\nabla U)^\top + \lambda I \operatorname{tr}(\nabla U) - (G + \lambda)\nabla U] \cdot \mathbf{n}}{2G + \lambda} \quad (24)$$

The implementation of this boundary condition is shown in Listing 5. Note that the `traction_` term in the code is the same as the f_{trac} mentioned in Equation (22). The additional `pressure_*n` term is used to specify a normal traction force on the boundary. In `bioFoam` [30], the pore pressure is subtracted from the gradient boundary in order to incorporate the effect of porous solid, whereas in this work, this pore pressure is not subtracted since the analytical solutions do not consider this effect.

```

1
2 void tractionDisplacementFvPatchVectorField::updateCoeffs()
3 {
4     if (updated())
5     {
6         return;
7     }
8
9     const fvPatchField<scalar>& mu =
10    patch().lookupPatchField<volScalarField, scalar>("mu");
11    const fvPatchField<scalar>& lambda =
12    patch().lookupPatchField<volScalarField, scalar>("lambda");
13
14    vectorField n = patch().nf(); //Unit normal
15
16    const fvPatchField<symmTensor>& sigmaD =
17    patch().lookupPatchField<volSymmTensorField,
18    symmTensor>("sigmaD");
19
20    gradient() =
21    (
22        (traction_ + pressure_*n)
23        + (2*mu + lambda)*fvPatchField<vector>::snGrad()
24        - (n & sigmaD)
25    ) / (2*mu + lambda);
26
27    fixedGradientFvPatchVectorField::updateCoeffs();
28 }
```

LISTING 5. Traction displacement

4. NUMERICAL EXAMPLES

To verify the implemented code, two different numerical examples are considered. In the first example, only Biot's consolidation equations are solved and the results of pore pressure and shear stress are compared with the analytical results in [5]. In the second example, Biot's consolidation equations and the pore pressure buildup equation (9) are solved to predict the onset of liquefaction. The numerical results are compared against Sumer's analytical results [4]. In addition to the two numerical examples, a new case is simulated to estimate the pore pressure buildup in a seabed with two columns. These three cases are discussed in detail in the following sections and are available for free download in the public repository [29].

4.1. Example 1: Pore pressure and shear stress verification. Hsu and Jeng [5] derived the analytical solution for the wave induced soil response in a realistic seabed. The authors present a semi-analytical approach to obtain solutions for the pore pressure and effective stresses in a non-cohesive layered seabed of finite thickness subject to a system of three-dimensional waves. To verify pore pressure and shear stress, `bioFoam` solver is used.

4.1.1. Boundary conditions: As mention in Section 3.3, at the mudline, Equation (20) is used to determine the wave-induced pore pressure. The traction free boundary condition is applied for the displacement. At the bottom of the seabed, zero pressure gradient and zero displacement are used. At the sides, periodic boundary conditions are used, i.e, pore pressure and displacement on the left side of the domain is equal to the respective pore pressure and displacement on the right side of the domain. The different boundary conditions are schematically depicted in the Figure 6.

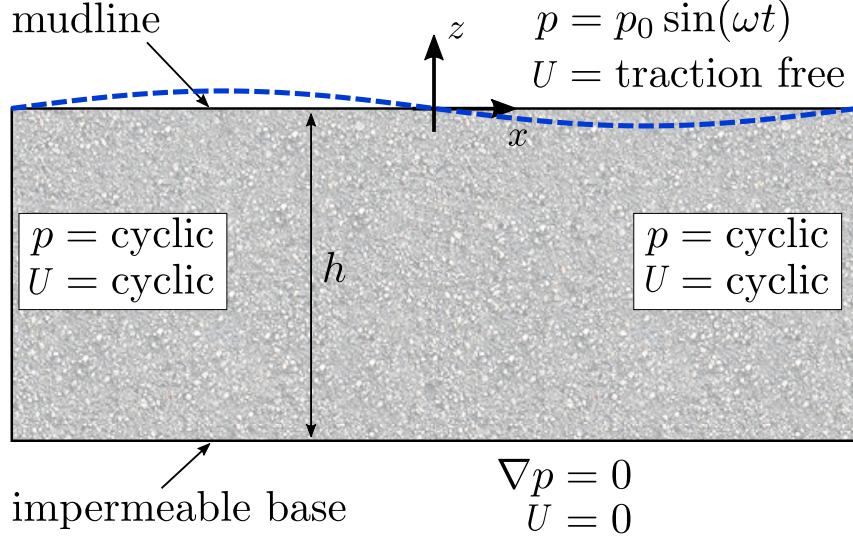


FIGURE 6. Schematic of the numerical domain including the boundary conditions applied for the pressure and displacement.

4.1.2. Model: A simple rectangular box is generated using OpenFOAM®'s `blockMesh` facility to represent the soil region. The length of the considered domain is equal to one wave length and the height is the same as that of the soil depth, h . Grid convergence study is conducted on the 2D grids to examine the convergence of the model using three different grid sizes: 50×25 , 100×50 and 200×100 . Figure 6 shows the grid convergence for the pore pressure and shear stress. Since, for grid size 100×50 and 200×100 , there is negligible difference between the results of the pore pressure and shear stress, a 2D mesh with 100 cells in x - direction and 50 cells in z - direction is used for the final simulation of Example 1. Similarly, for the convergence study on the temporal discretisation, three different time steps are considered: $t = 0.05$ s, $t = 0.1$ s and $t = 0.2$ s. The difference in the results are negligible. Therefore, the time step $t = 0.2$ s is considered for all remaining simulations. For the sake of brevity, plots of the pore pressure or shear stress are omitted for the temporal convergence study. The wave and seabed parameters used for this numerical model are adapted from Hsu and Jeng [5] and are listed in Table 1. The amplitude of the pressure in Equation (20) can be derived based on the water density, water depth, wave height, and wave length

$$A_p = \frac{\gamma_w H}{2 \cdot \cosh(\frac{2\pi}{L} \cdot d)} = 18640.55 \text{ N m}^{-2} \quad (25)$$

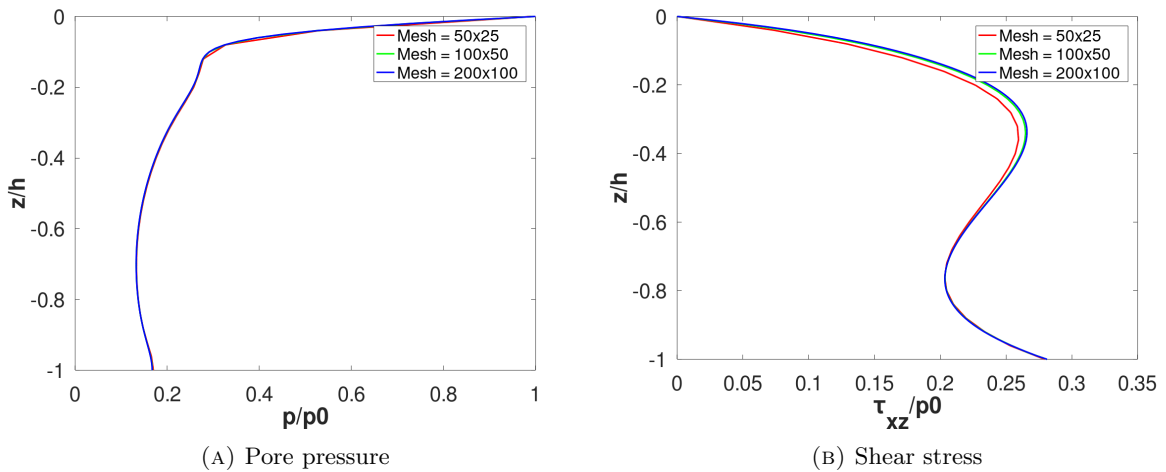
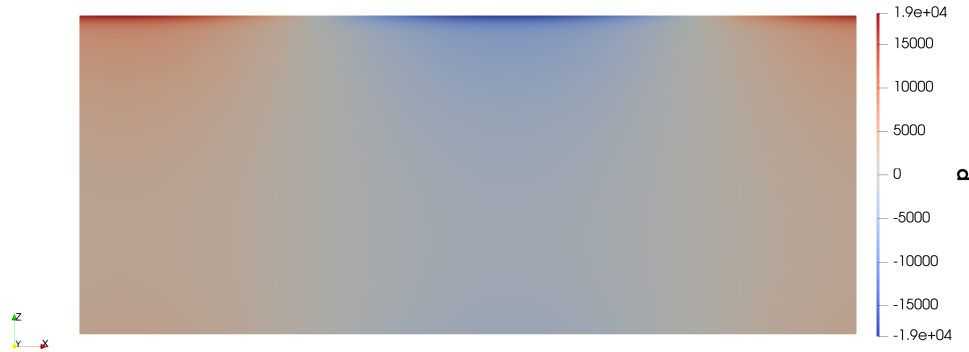
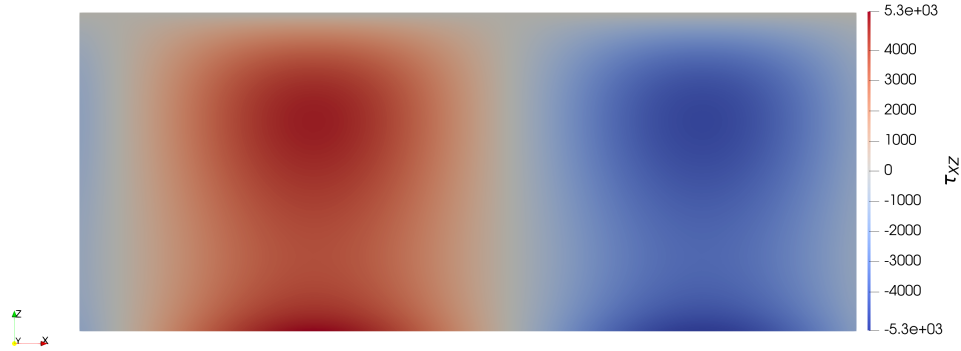


FIGURE 7. Grid convergence study with three different grid resolutions for pore pressure (A) and shear stress (B)

TABLE 1. Physical properties of the wave and seabed for the model validation

| Physical property | Value | Unit |
|--------------------------|------------------------|------------|
| Wave parameters | | |
| Water depth | $d = 20$ | m |
| Wave height | $H = 6$ | m |
| Wave period | $T = 10$ | s |
| Wave length | $L = 122.025$ | m |
| Seabed parameters | | |
| Soil depth | $h = 50$ | m |
| Poisson ratio | $\nu = 0.333$ | — |
| Porosity | $n = 0.3$ | — |
| Saturation | $S_r = 0.975$ | — |
| Young Modulus | $E = 2.67 \times 10^7$ | $N m^{-2}$ |
| Permeability | $k = 0.001$ | $m s^{-1}$ |
| Bulk Modulus | $K = 2 \times 10^9$ | $N m^{-2}$ |

(A) Pore pressure ($N m^{-2}$)(B) Shear stress ($N m^{-2}$)FIGURE 8. Numerical results of the pore pressure and shear stress at time $t = 25$ s

4.1.3. Results: In order to validate the numerical model, the results of pore pressure and shear stress are compared against Hsu and Jeng's analytical solution [16]. Figure 8 shows the numerical results of pore pressure and shear stress at time $t = 25$ s. Figure 9a shows the results of the normalised pore pressure (p/p_0) along the soil depth (z/h). Similarly, Figure 9b shows the results of normalized shear stress against

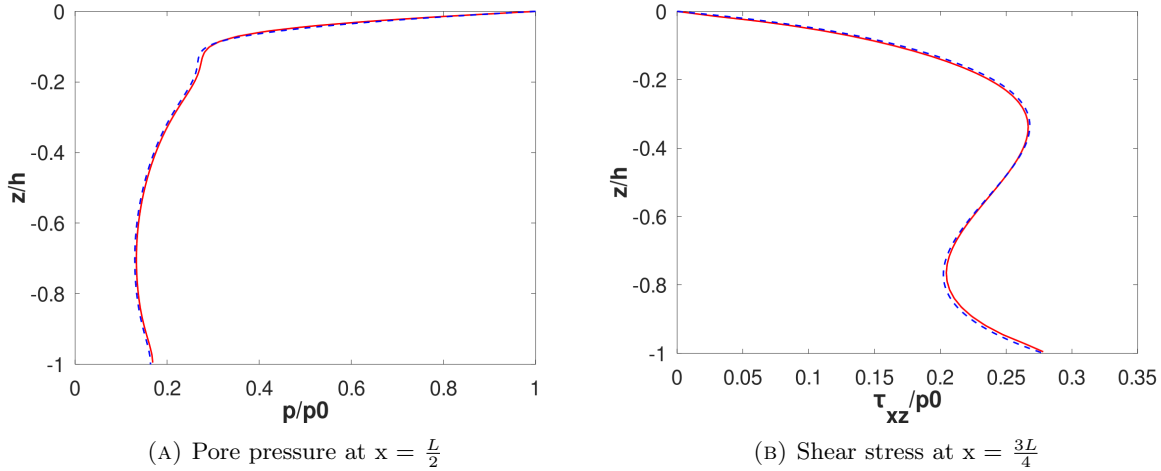


FIGURE 9. Comparison of analytical (dashed line) and numerical results at time $t = 25$ s (solid line) of the pore pressure (A) and shear stress (B) of Example 1

normalized soil depth. The pore pressure and shear stress are determined using OpenFOAM® function object `sampling` with interpolation scheme `cellPointFace`, which calculates the values of fields for a specified range. Also, one can specify the number of sampling points required in the specified range. The results show that the pore pressure is maximum at the mudline due to the direct contact with the wave. The non-linearity of the pressure along the soil depth is due to the soil properties. For quantitative analysis, the Mean Absolute Percentage Error (MAPE) (see Equation (26)) is evaluated.

$$\text{MAPE} = \frac{1}{j} \cdot \sum_{i=1}^j \left(\frac{|x_r - x_p|}{|x_r|} \right)_i \quad (26)$$

In Equation (26), j denotes the number of sampling points. x_r and x_p are the reference and the predicted value, respectively. For pore pressure and shear stress, errors are found to be 2.5% and 1.7%, respectively. These results indicate that the numerical results of pore pressure and shear stress are in good agreement with the analytical results.

4.2. Example 2: Onset of liquefaction. As mentioned in Section 2.2, to estimate the accumulated pore pressure the rearrangement of soil grains has to be taken into account, for which the additional Equation (9) for pore pressure buildup is solved. Since the amplitude of shear stress is not accurate initially, `biotFoam` is simulated first and using the amplitude of shear stress from the `biotFoam`, `pressureBuildupFoam` is used. In order to validate onset of liquefaction, the results from the present numerical model are compared against analytical solutions of Sumer [4].

4.2.1. Model: Similar to the previous example, a simple rectangular box with length equal to one wave length and height equal to the soil depth is generated using OpenFOAM®'s `blockMesh` facility to represent the soil region. The mesh generated is a 2D mesh with 100 cells in x -direction and 50 cells in z -direction. The time step is $t = 0.2$ s. The parameters used for this numerical model are adapted from Sumer [4] and are listed in Table 2. Using Equation (25), and based on the wave parameters in Table 2, the amplitude of the pressure can be calculated as $23643.45 \text{ N m}^{-2}$. It is worth to note that the values of α and β are taken from McDougal *et al.* [34], and they represent the soil in their experiment with $D_r = 0.54$. These values are slightly different from those obtained through the empirical equation given in Equation (17) for the same relative density $D_r = 0.54$. The original values given in [34], and reproduced in Sumer [4] are maintained here to avoid confusion.

4.2.2. Boundary conditions: For solving `biotFoam`, the same boundary types are used as in the previous example. To solve for `pressureBuildupFoam`, boundary conditions for the accumulated pore pressure (P) are required. P is zero at the seabed, zero gradient at the seabed bottom, and cyclic at the sides. The different boundary conditions are schematically depicted in the Figure 10.

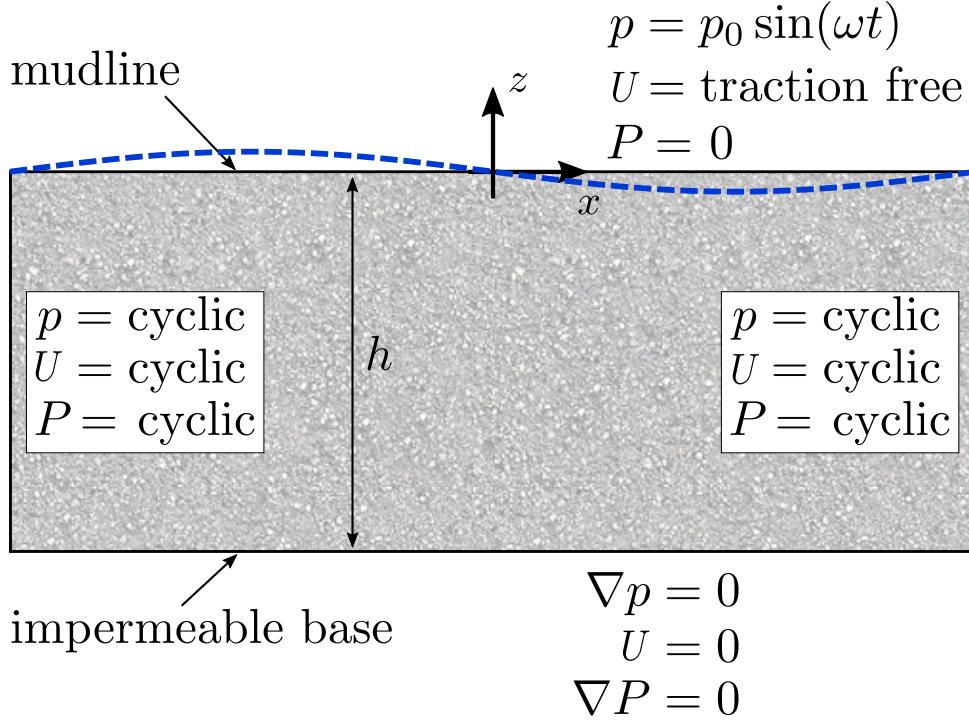


FIGURE 10. Schematic of the numerical domain including the boundary conditions applied for the pressure, accumulated pore pressure, and displacement.

TABLE 2. Physical properties of the wave and seabed for model validation

| Physical property | Value | Unit |
|---------------------------------------|--------------------------------------|----------------------------|
| Wave parameters | | |
| Water depth | $d = 19$ | m |
| Wave Height | $H = 6$ | m |
| Wave period | $T = 13.7$ | s |
| Wave length | $L = 174$ | m |
| Seabed parameters | | |
| Soil depth | $h = 1$ | m |
| Poisson ratio | $\nu = 0.35$ | — |
| Porosity | $n = 1/3$ | — |
| Saturation | $S_r = 1$ | — |
| Modulus | $E = 2.5 \times 10^6$ | N m^{-2} |
| Permeability | $k = 10^{-6}$ | m s^{-1} |
| Bulk Modulus | $K = 1.9 \times 10^9$ | N m^{-2} |
| Pressure buildup parameters | | |
| Coefficients | $\alpha = 0.246$ $\beta = -0.165$ | — |
| Relative density | $D_r = 0.54$ | — |
| Coefficient of lateral earth pressure | $k_0 = 0.4$ | — |
| Coefficient of consolidation | $c_v = 4.1 \times 10^{-4}$ | $\text{m}^2 \text{s}^{-1}$ |

4.2.3. Results: In the first simulation, `biotFoam` is used and using OpenFOAM® function object `Prime2Mean` the root-mean-square is calculated and later the amplitude of the shear stress (A_τ). This simulation is continued until 15 minutes simulated time in order to have the steady and accurate shear stress. Now, `pressureBuildupFoam` is simulated to solve the pressure build up equation. Here, the source term is calculated using A_τ from `biotFoam`. Figure 11 shows the time evolution of accumulated pore pressure at five different soil depths. Figure 12 shows the numerical results of liquefaction criteria after 15 minutes. In Figure 12, the region is completely liquefied. Figure 13 shows the liquefaction criteria plotted against the normalized soil depth and is validated against the analytical solution. The liquefaction criterion

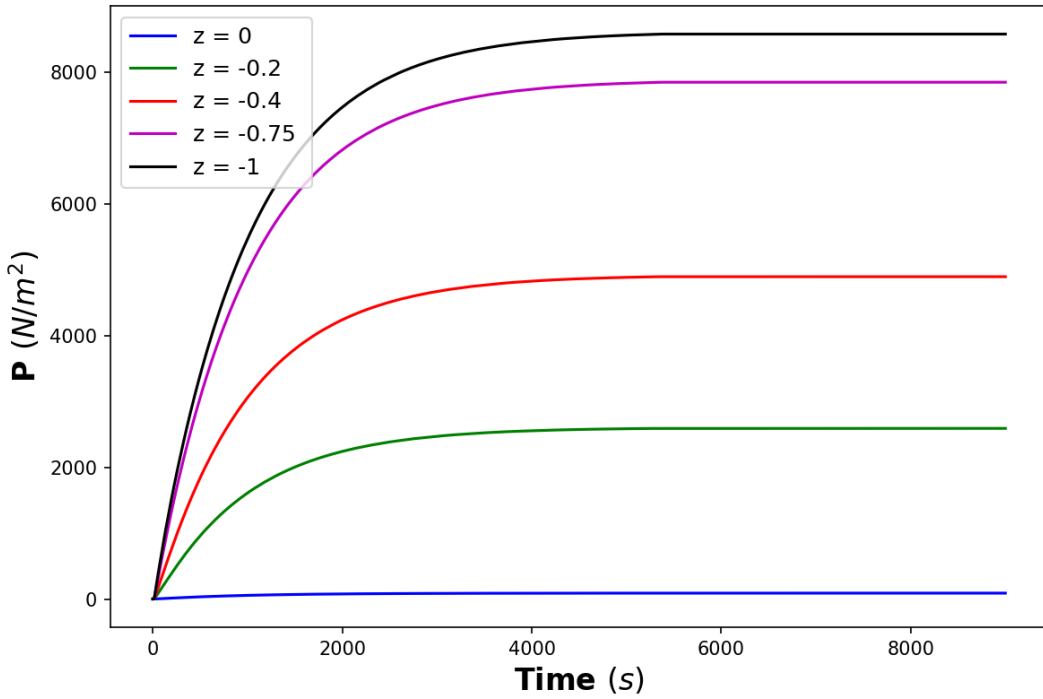


FIGURE 11. Progress of accumulated pore pressure at different soil depths for Example 2.



FIGURE 12. Numerical results of liquefaction criteria after 15 minutes of Example 2 (exaggerated z -axis). The red and blue colors indicate the liquefied and non-liquefied regions, respectively.

(P/σ'_0) is obtained using OpenFOAM® function object sampling as described in the previous example. As time progresses, the liquefaction criteria gradually increases and reaches unity. After 15 minutes, the top part of the seabed ($z/h > -0.6$) is completely liquefied. [35] emphasized that small error in shear stress may lead to larger error in the pore pressure buildup. Therefore, the deviation of the numerical results in Figure 13 may be due to inaccurate calculation of the mean shear stress from the instantaneous values. Also, the analytical solutions are solved using frequency domain and the numerical solutions are solved using the time domain. The main objective of this work is to determine the onset of liquefaction in

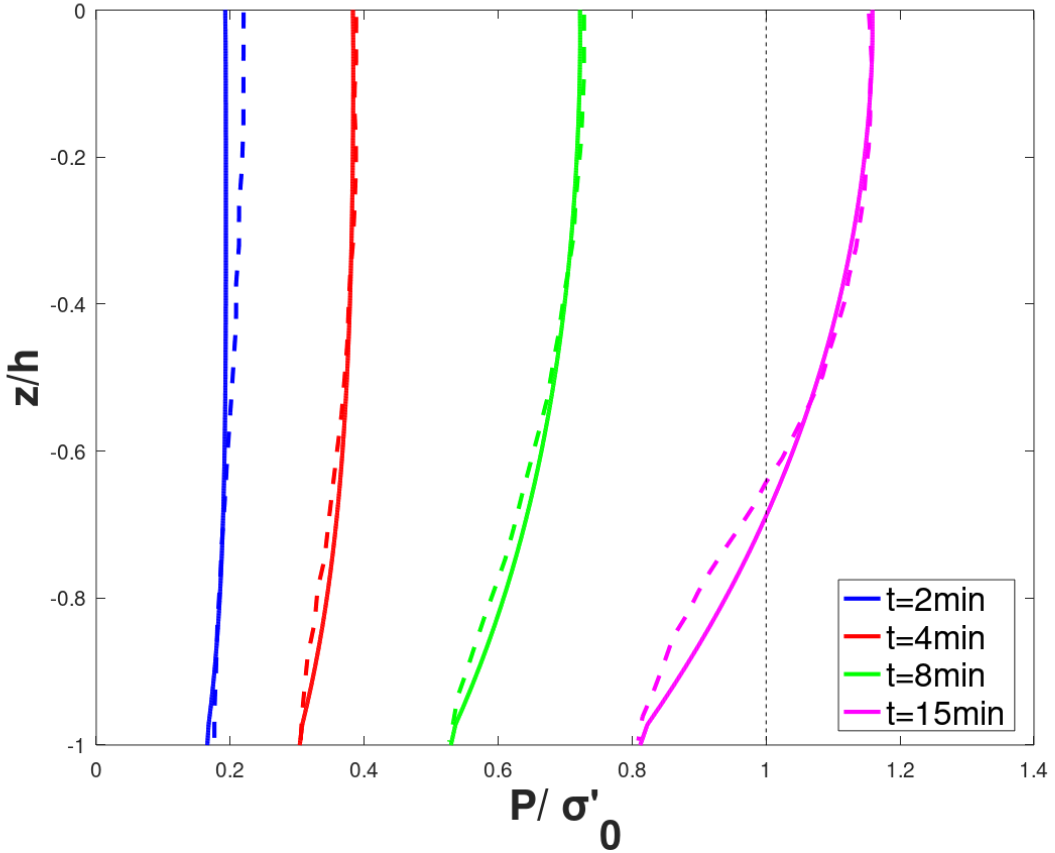


FIGURE 13. Comparison of the analytical (dashed lines) and numerical (solid lines) results for the normalised accumulated pore pressure at four different time instances, i.e. 2, 4, 8, and 15 min. The vertical dotted line at $P/\sigma'_0 = 1$ indicates the liquefaction criteria. For $P/\sigma'_0 > 1$ liquefaction sets in. The analytical values are digitized from Sumer's [4] analytical solution.

order to solve different constitutive equations for the liquefied soil. Therefore, more attention was payed to the accurate prediction of the onset of liquefaction.

4.3. Example 3: Seabed with stone column. After the excellent agreement of numerical accumulated pore pressure results with the analytical results, Example 2 is extended to predict onset of liquefaction for a seabed with stone column.

Stone columns are essentially an array of crushed stone pillars placed into the soil in a regular or staggered grid, possibly with a vibrating tool [36]. They can either be used below a proposed structure for ground improvement, or for the stability of a loose marine deposit. The stone column technique of ground treatment has proven successful in

- (1) improving slope stability of both embankments and natural slopes,
- (2) increasing bearing capacity,
- (3) reducing total and differential settlements (i.e. the spatially uneven settlement of a structure's foundation, which may lead to structural damage),
- (4) reducing the liquefaction potential of silt or fine sand deposits and
- (5) increasing the time rate of settlement.

A good example for item (4) usage above is the ground improvement for a runway of Haneda Airport (Tokyo, Japan) [37].

4.3.1. Model: The mesh used in this example is the same as Example 2 i.e, a 2D mesh with 100 cells in x - direction and 50 cells in z - direction. The stone column is considered for the entire cell in z - direction and for 25th, 50th, 51st and 76th cells in x - direction. The parameters used for this numerical model in

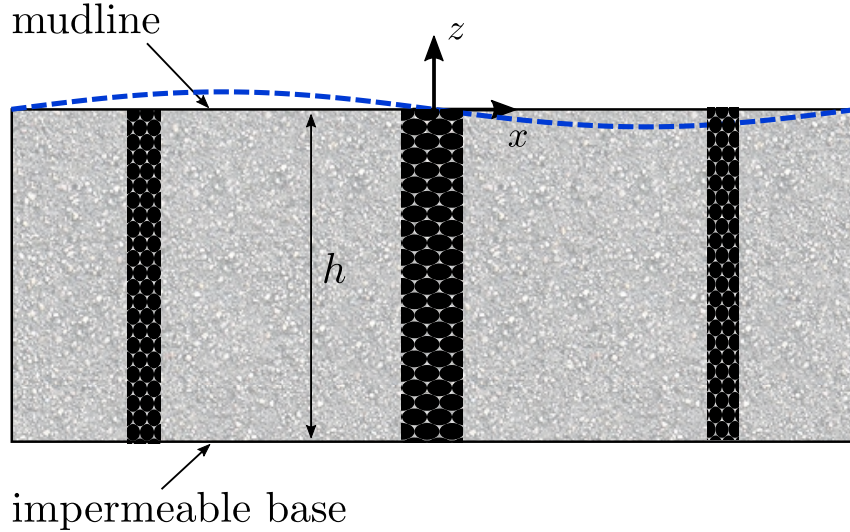


FIGURE 14. Schematic of the numerical domain including the boundary conditions applied for the pressure and displacement for Example 3

TABLE 3. Physical properties changed for the stone column

| Physical property | Value | Unit |
|-------------------|---------------------|-------------------|
| Poisson ratio | $\nu = 0.33$ | — |
| Porosity | $n = 0.32$ | — |
| Modulus | $E = 2 \times 10^7$ | N m^{-2} |
| Permeability | $k = 10^{-2}$ | m s^{-1} |

the stone columns are listed in Table 3 and the rest of the region are same as in 2. Figure 14 shows the schematic representation of seabed with two stone column.

4.3.2. *Boundary conditions:* The same boundary conditions are used as in Example 2.

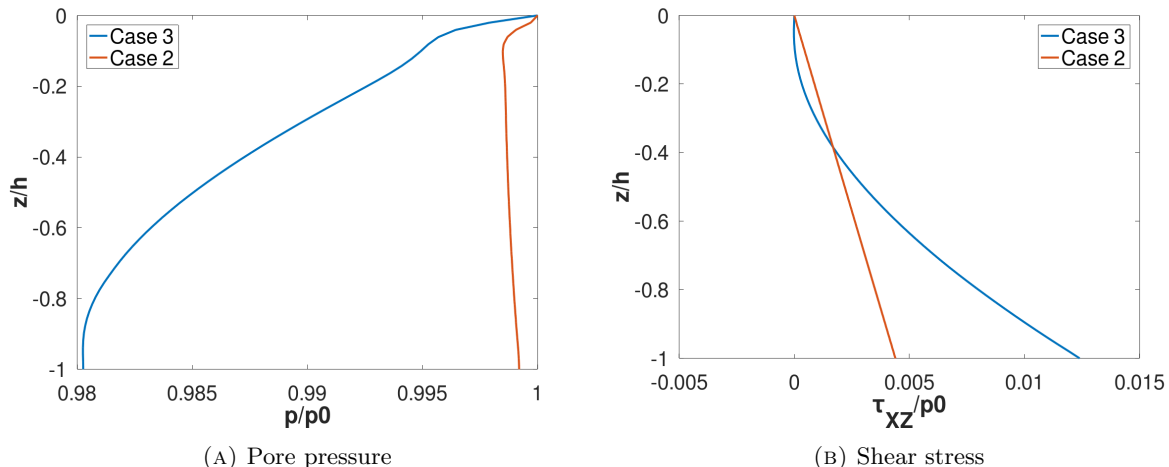


FIGURE 15. Numerical results of pore pressure and shear stress near the stone column at $x = 84$ m

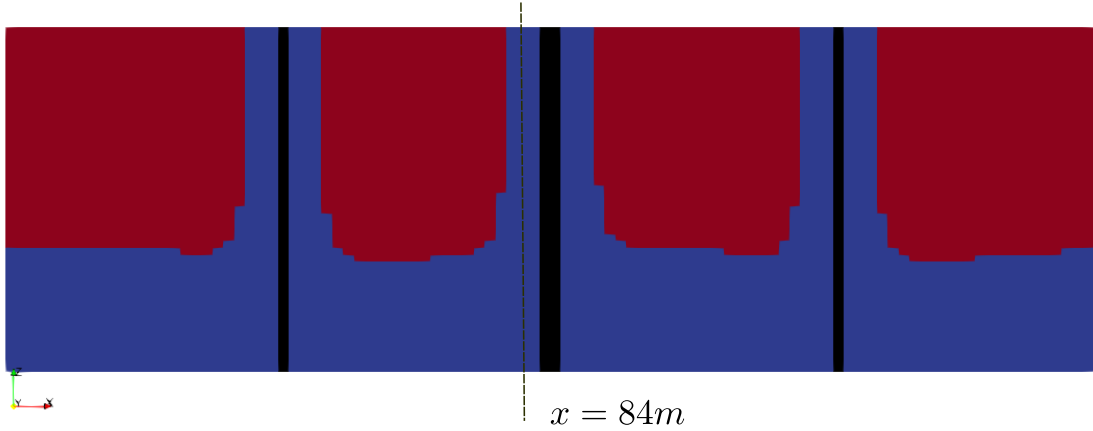


FIGURE 16. Numerical results of liquefaction criteria after 15 minutes of Example 3 (exaggerated z -axis). The red, blue and black colors indicate liquefied, non-liquefied and stone column regions, respectively.

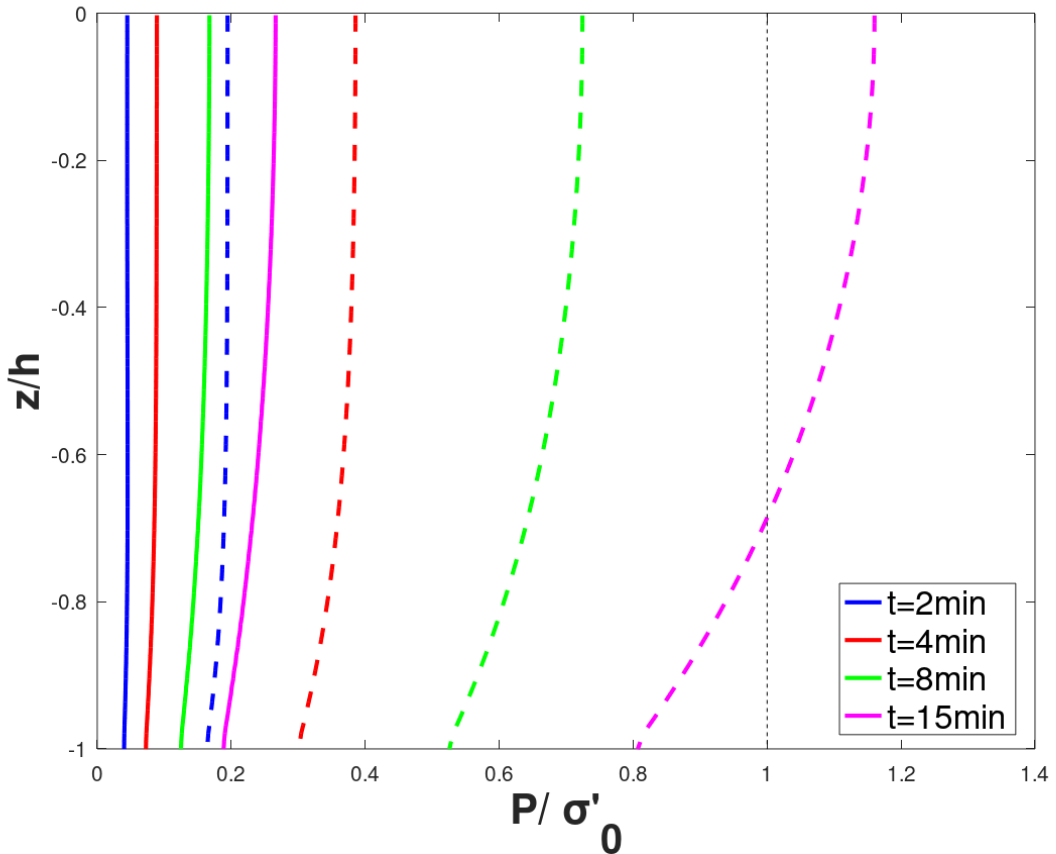


FIGURE 17. Comparison of the numerical results of seabed without stone column (dashed lines) and with stone column (solid lines) for the normalised accumulated pore pressure at four different time instances, i.e. 2, 4, 8, and 15 min for $x = 84\text{ m}$.

4.3.3. Results: The properties of the seabed are varied using OpenFOAM® dictionary `setField`. Similar to the previous example, `biotFoam` is initially simulated to calculate the root-mean-square of the

shear stress. This value is used in `pressureBuildupFoam` to calculate the accumulated pore pressure and the liquefaction criteria. The properties of the stone column are described in Table 3. The stone column acts as drainage and there is no accumulation of pressure. Figure 15 shows the comparison of numerical results of pore pressure and shear stress of case 2 and case 3 at $x = 84$ m. The source term f is set to zero in that region. In this case, the liquefaction begins after time $t = 730$ s, whereas in the Example 2, at the same time, $z/h > -0.15$ of the seabed is already liquefied. Figure 16 shows that there is no liquefaction near the stone column due to the drainage effects and away from the stone column, the liquefaction is high and is almost the same as the liquefaction depth in Example 2. The amount of accumulation of pore pressure near the second stone column at four different time instances for $x = 84$ m is shown in Figure 17. Since, the simulation is in 2D, the stone column behaves like a stone wall. This limits the displacement of neighbouring silt significantly, causing higher shear stress than the stone column. In this specific case, a representative 2D example is modelled. Figure 17 show that liquefaction depth as well as the extent of liquefaction is reduced with the introduction of stone columns. Furthermore, as shown in Figure 16 near the location of the stone column, liquefaction is prevented. The decrease in liquefaction near the stone columns is due to the high porosity and permeability of stone columns which causes the pore pressure to dissipate faster than it is accumulated. This example can be transferred to 3D which induces high shear stress only locally around the stone column.

5. CONCLUSIONS AND SUGGESTIONS FOR FUTURE WORK

In this study, the wave induced seabed response in terms of pore pressure variations have been investigated. The numerical results of pore pressure and shear stress show good agreement compared with the analytical solutions of Hsu and Jeng [5]. To estimate the residual liquefaction, a criterion based on accumulated pore pressure has been used. To calculate the accumulated pore pressure, a laplacian equation is solved with the source term based on amplitude of shear stress. A novel technique has been implemented in OpenFOAM® to calculate the aforementioned amplitude of shear stress from the root-mean-square of the shear stress. The numerical results of the accumulated pore pressure also shows good agreement compared with Sumer's analytical solution [4]. On calculating the liquefaction criteria of the seabed with the stone column, the liquefaction potential reduced towards the stone column and far from the stone column, the effects are no longer seen. In future, simulations can be performed with more number of stone columns and different material properties for the stone column to have better drainage properties and delay the liquefaction. Also, this case can be extended to 3D to limit the high shear stress only around the stone column.

In this study, the first steps towards a numerical, OpenFOAM®-based, modeling tool for the analysis of seabed liquefaction around marine structures are presented. In the future, this study will be extended including a more complete representation of the hydro-geotechnical processes by, e.g., simulating the liquefied soil with different constitutive relations until it reaches compaction. Further extensions of the model could include the detailed representation of the free surface interface.

ACKNOWLEDGEMENTS

NuLIMAS receives funding through the ERA-NET Cofund MarTERA (Grant No. 728053) in the H2020 framework. Funding is also received from the German Federal Ministry for Economic Affairs and Climate Action (Grant No. 03SX524A), the Scientific and Technological Research Council of Turkey (Grant No. TEYDEB-1509/9190068), and the Polish National Centre for Research and Development (Grant MarTERA-2/NuLIMAS/3/2021).

Author Contributions: Conceptualisation, H.R., Ö.K. and M.S.; methodology, H.R., Ö.K. and M.S.; software, R.S and H.R.; validation, R.S. and H.R.; formal analysis, n.a.; investigation, R.S. and H.R.; resources, H.R., Ö.K. and M.S.; data curation, R.S. and H.R.; writing—original draft preparation, R.S. and C.W.; writing—review and editing, R.S., H.R., C.W., N.G., Ö.K. and M.S.; visualisation, R.S.; supervision, H.R., C.W. and N.G.; project administration, C.W. and N.G.; funding acquisition, H.R., Ö.K., M.S. and N.G. All authors have read and agreed to the published version of the manuscript.

REFERENCES

- [1] R. M. Aydenlou, "Chapter five - Site pathology and seismic rehabilitation methods," in *Seismic Rehabilitation Methods for Existing Buildings*, R. M. Aydenlou, Ed. Butterworth-Heinemann, 2020, pp. 593–636.
- [2] Y. Huang, Y. Bao, M. Zhang, C. Liu, and P. Lu, "Analysis of the mechanism of seabed liquefaction induced by waves and related seabed protection," *Natural Hazards*, vol. 79, no. 2, pp. 1399–1408, 2015.
- [3] NASA earth observatory, *Squeezing Water from Rock*, 2003, <https://earthobservatory.nasa.gov/features/Earthquake>, Last accessed 22/08/2021.
- [4] B. Mutlu Sumer, *Liquefaction Around Marine Structures*. World scientific, 2014, vol. 39.

- [5] J. R. C. Hsu and D. S. Jeng, "Wave-induced soil response in an unsaturated anisotropic seabed of finite thickness," *International Journal for Numerical and Analytical Methods in Geomechanics*, vol. 18, no. 11, pp. 785–807.
- [6] J. T. Christian, P. K. Taylor, J. K. Yen, and D. R. Erali, "Large diameter underwater pipe line for nuclear power plant designed against soil liquefaction," in *Offshore technology conference*. OnePetro, 1974.
- [7] H. Lundgren, J. Lindhardt, and C. Romhild, "Stability of breakwaters on porous foundation," *12th International Conference on Soil Mechanics and Foundation Engineering*, vol. 1, pp. 451–454, 1973.
- [8] B. M. Sumer and V. S. O. Kirca, "Scour and liquefaction issues for anchors and other subsea structures in floating offshore wind farms: A review," *Water Science and Engineering*, 2021.
- [9] P. K. Esfeh and A. M. Kaynia, "Numerical modeling of liquefaction and its impact on anchor piles for floating offshore structures," *Soil Dynamics and Earthquake Engineering*, vol. 127, p. 105839, 2019.
- [10] F. Adam, C. Steinke, F. Dahlhaus, J. Großmann et al., "Gicon®-tlp for wind turbines—validation of calculated results," in *in the Proceedings of The Twenty-Third International Offshore and Polar Engineering Conference, Anchorage, Alaska, USA*. International Society of Offshore and Polar Engineers, 2013, pp. 1–7.
- [11] GICON®, *Project website of the GICON SOF*, 2021, <http://www.gicon-sof.de/en/sof1.html>, Last accessed 22/01/2021.
- [12] M. Stapelfeldt, B. Bienen, and J. Grabe, "The influence of the drainage regime on the installation and the response to vertical cyclic loading of suction caissons in dense sand," *Ocean Engineering*, vol. 215, 2020.
- [13] M. A. Biot, "General theory of three-dimensional consolidation," *Journal of applied physics*, vol. 12, no. 2, pp. 155–164, 1941.
- [14] T. Yamamoto, H. Koning, H. Sellmeijer, and E. Van Hijum, "On the response of a poro-elastic bed to water waves," *Journal of Fluid Mechanics*, vol. 87, no. 1, pp. 193–206, 1978.
- [15] O. Madsen, "Wave-induced pore pressures and effective stresses in a porous bed," *Geotechnique*, vol. 28, no. 4, pp. 377–393, 1978.
- [16] J. R. C. Hsu and D. S. Jeng, "Wave-induced soil response in an unsaturated anisotropic seabed of finite thickness," *International Journal for Numerical and Analytical Methods in Geomechanics*, vol. 18, no. 11, pp. 785–807, 1994.
- [17] B. M. Sumer and N.-S. Cheng, "A random-walk model for pore pressure accumulation in marine soils," in *The Ninth International Offshore and Polar Engineering Conference*. OnePetro, 1999.
- [18] D. S. Jeng, "Wave-induced sea floor dynamics," *Appl. Mech. Rev.*, vol. 56, no. 4, pp. 407–429, 2003.
- [19] H. Elsafti and H. Oumeraci, "A numerical hydro-geotechnical model for marine gravity structures," *Computers and Geotechnics*, vol. 79, pp. 105–129, 2016.
- [20] Y. Li, M. C. Ong, and T. Tang, "A numerical toolbox for wave-induced seabed response analysis around marine structures in the openfoam®," *Ocean Engineering*, vol. 195, p. 106678, 2020.
- [21] Y. Li, M. C. Ong, and D. R. Fuhrman, "Cfd investigations of scour beneath a submarine pipeline with the effect of upward seepage," *Coastal Engineering*, vol. 156, p. 103624, 2020.
- [22] N. G. Jacobsen, D. R. Fuhrman, and J. Fredsøe, "A wave generation toolbox for the open-source CFD library: OpenFoam®," *International Journal for numerical methods in fluids*, vol. 70, no. 9, pp. 1073–1088, 2012.
- [23] L. Duan and D. Wang, "Novel three-dimensional numerical model for residual seabed response to natural loadings near a single pile," *Applied Ocean Research*, vol. 94, p. 102004, 2020.
- [24] L. Duan, D.-S. Jeng, and D. Wang, "Poro-fssi-foam: Seabed response around a mono-pile under natural loadings," *Ocean Engineering*, vol. 184, pp. 239–254, 2019.
- [25] T. Sui, C. Zhang, D.-s. Jeng, Y. Guo, J. Zheng, W. Zhang, and J. Shi, "Wave-induced seabed residual response and liquefaction around a mono-pile foundation with various embedded depth," *Ocean Engineering*, vol. 173, pp. 157–173, 2019.
- [26] W. H. Peacock and H. B. Seed, "Sand liquefaction under cyclic loading simple shear conditions," *Journal of the Soil Mechanics and Foundations Division*, vol. 94, no. 3, pp. 689–708, 1968.
- [27] P. A. De Alba, C. K. Chan, and H. B. Seed, "Sand liquefaction in large-scale simple shear tests," *Journal of the Geotechnical Engineering Division*, vol. 102, no. 9, pp. 909–927, 1976.
- [28] B. M. Sumer, V. S. O. Kirca, J. Fredsøe et al., "Experimental validation of a mathematical model for seabed liquefaction under waves," *International Journal of Offshore and Polar Engineering*, vol. 22, no. 02, 2012.
- [29] "pressurebuildupfoam," <https://github.com/NuLIMAS/pressureBuildupFoam>, 2021.
- [30] J. Roenby, "Openfoam library for soil mechanics," <https://github.com/roenby/soilFoam>, 2013.
- [31] Ž. Tuković, A. Ivanković, and A. Karač, "Finite-volume stress analysis in multi-material linear elastic body," *International journal for numerical methods in engineering*, vol. 93, no. 4, pp. 400–419, 2013.
- [32] T. Tang, "Modeling of soil-water-structure interaction," 2014.
- [33] T. Tang, F. Vesting, and J. Andric, "Implementation of solid body stress analysis in openfoam," *Report for the course "CFD with OpenSource software" held at Chalmers University of Technology*, 2012.
- [34] W. McDougal, Y. Tsai, P. L. Liu, and E. Clukey, "Wave-induced pore water pressure accumulation in marine soils," 1989.
- [35] L. Cheng, B. M. Sumer, and J. Fredsøe, "Solutions of pore pressure build up due to progressive waves," *International journal for numerical and analytical methods in geomechanics*, vol. 25, no. 9, pp. 885–907, 2001.
- [36] G. Billoet&J and R. Gauthey, "Recommendations for the design, calculation, construction and quality control of stone columns under buildings and sensitive structures," *USG, the French geotechnical union association Version No.*
- [37] "Stone Columns Projects," <https://jafecusa.com/projects/stone-columns/>, accessed: 2021-09-20.

6. APPENDIX

The terms in the code that are denoted different from the theoretical description are tabulated in Table 4.

TABLE 4. Conversion table

| Description | Code | Theory |
|-----------------------------------|--------|-------------|
| Displacement | D | U |
| Accumulated pore pressure | pE | P |
| Stress | sigmaD | σ |
| Velocity | U | V |
| Shear modulus | mu | G |
| Specific weight of soil | gammaD | γ' |
| Coefficient of consolidation | cv | c_v |
| constant | Dp1 | n/K' |
| constant | Dp2 | k/γ |
| constant | Dp3 | 1 |
| Number of cycles for liquefaction | numCyc | N_l |
| Initial effective stress | sigma0 | σ'_0 |
| Amplitude of shear stress | tauAmp | A_τ |